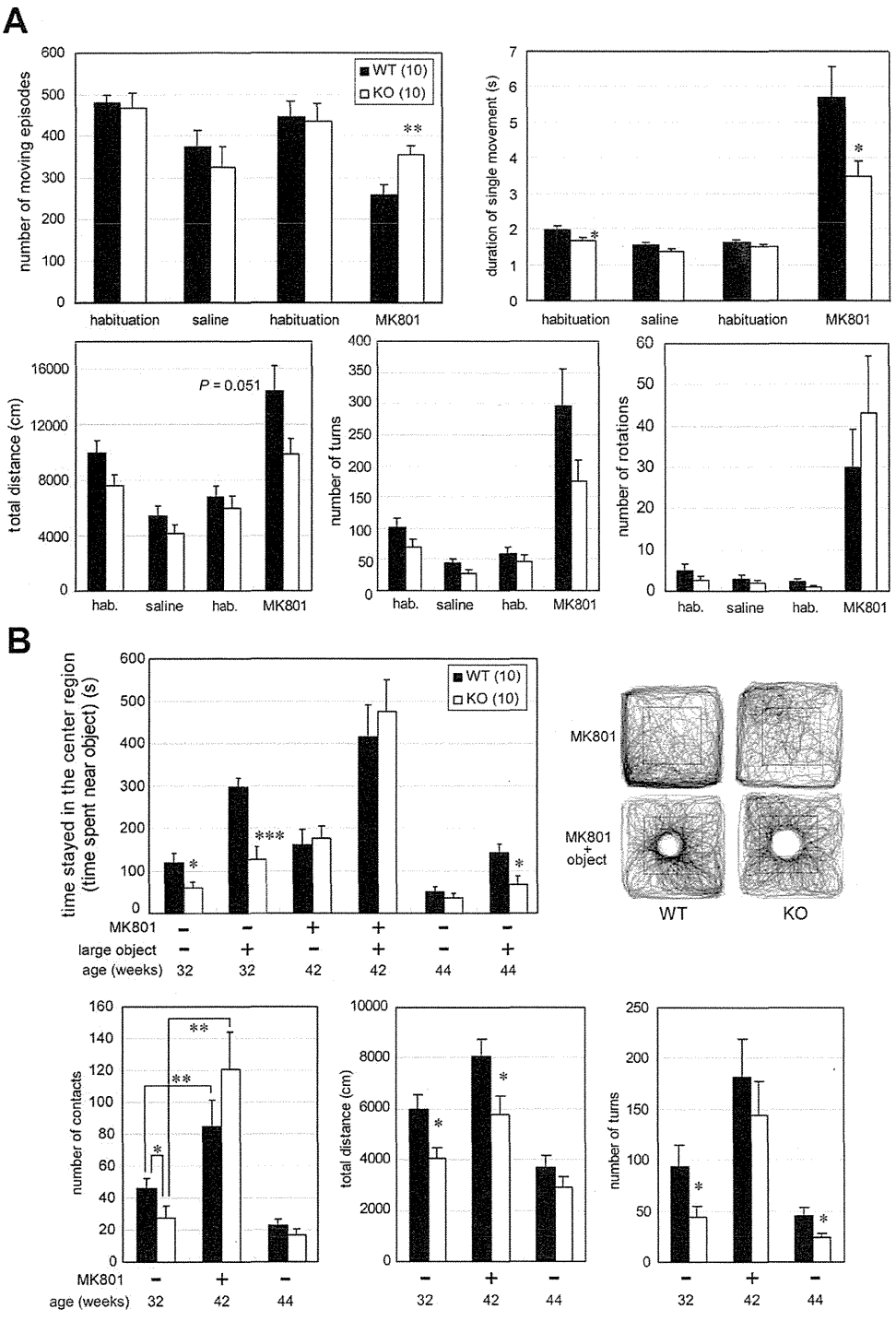

Figure 7. Effects of MK-801 administration on *Lrrtm1* KO behavior in the OF box. (A) Locomotor activities before (habituation) and 10 min after MK-801 treatment or saline treatment were examined in the OF apparatus. Saline injection was done once, followed by MK-801 injection the next day, using the same animals. Number of moving episodes, duration of a single movement, total distance, number of turns, and number of rotations were measured in each 30-min session. (B) Approach to the large object. (*top left*) Time spent in the central area (30% of the total area, indicated as squares in the representative traces at *top right*), which included the large, inanimate object, in the 15-min test period. Compare the traces with those in Figure 3A. As a control, we used the value of the latter half (15 min) of the preceding OF session (large object [–]). (*bottom*) Number of contacts with the large object before, soon after, and 2 weeks after MK-801 treatment. As controls, corresponding values in the large inanimate object approach test (Figure 3A) are indicated (*MK801-, 32 weeks*). The experiments were done in the same animals at the ages indicated. Values are presented as means ±SEM. * $P<0.05$; ** $P<0.01$, *** $P<0.001$.
doi:10.1371/journal.pone.0022716.g007

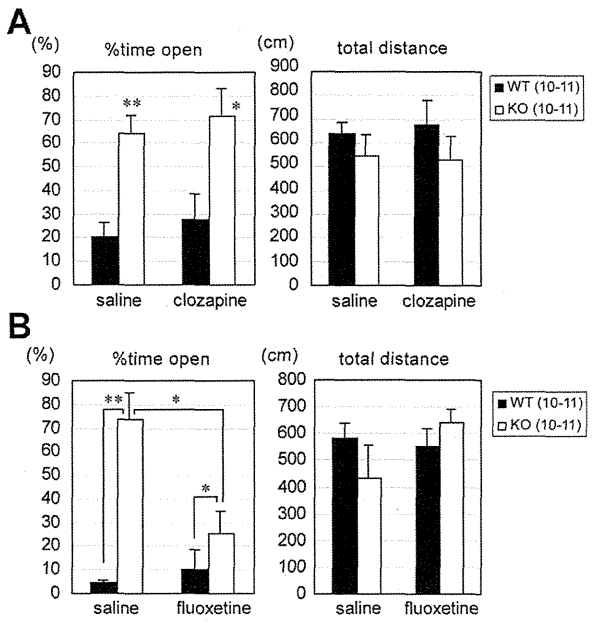

Figure 8. Effects of clozapine or fluoxetine administration on *Lrrtm1* KO behavior in the elevated plus maze test. (A, B) Percentage of time spent in the open arms and total distance traveled in the elevated plus maze test. WT and KO mice were subjected to the test 30 min after intraperitoneal injection of saline, 0.4 mg/kg clozapine, or 10 mg/kg fluoxetine. (A) clozapine treatment. (B) fluoxetine treatment. Values are presented as means ±SEM. * $P<0.05$; ** $P<0.01$ in U-test.
doi:10.1371/journal.pone.0022716.g008

from the afternoon of the day of transfer to the behavioral laboratory (Day 1) until the first day of the next week (Day 8). After the termination of home-cage activity measurement, cages and bedding materials were changed to fresh ones and the mice were maintained in the same type of micro-isolation rack (Allentown Inc., Allentown, NJ, USA) as used in the breeding rooms throughout the behavioral screening.

OF test

The OF test was performed as previously described [29]. Each mouse was placed in the center of an OF apparatus [50×50×40 (H) cm] illuminated by light-emitting diodes (LEDs; 70 lx at the center of the field) and then allowed to move freely for 15 min. Distance traveled (cm) and time spent (%) in the central area of the field (30% of the field) or in the four corner squares of the 5×5 subdivisions were adopted as indices, and the relevant data were collected every 1 min. Data were collected and analyzed by using Image J OF4 (O'Hara).

Hole-board test

An OF system made of gray plastic (50×50×40 (H) cm) with four equally separated holes (3 cm diameter with infra-red sensor) on the floor was used (Model ST-1/WII, Muromachi-kikai, Tokyo, Japan). The field was illuminated by fluorescent light (180 lx, at the center of the field), and the level of background noise was approximately 50 dB. The behavior of each mouse was monitored by a CCD camera located about 1.5 m above the field. In the HB test, mice were individually introduced into the center of the field and were then allowed to explore freely for 5 min. Total moving time (s), distance traveled (cm), latency of head-dipping (s), number of head-dips, duration of head-dipping (s), duration of rearing (s), and number of rearings were measured as indices. Data were collected and analyzed by using a CompACT VAS system (Muromachi-Kikai, Tokyo, Japan).

Light–dark box test

A four-channel LD-box system was added to the same soundproof room as the OF. Each light box was made of white plastic [20×20×20 (H) cm] and illuminated by LEDs (250 lx at the center of the box); a CCD camera was attached to the ceiling. Each dark box was made of black plastic [20×20×20 (H) cm]; an infrared camera was attached to the ceiling. There was a tunnel for transition on the center panel between the light box and dark box (3×5 cm) via a sliding door. In the LD test, mice were individually introduced into the light box, and the door of the tunnel automatically opened immediately after the software detected the mouse. The mice were then allowed to move freely in the LD box for 10 min. Total distance traveled, percentage of time spent in the light box, number of transitions between the light and dark boxes, and the duration of the first latency period before entry to the dark box were measured as indices. Data were collected and analyzed by using Image J LD4 (O'Hara).

Elevated plus maze test

A single channel of EPM [closed arms: 25×5×15 cm (H); open arms 25×5×0.3 cm (H)) was placed in the same soundproof room that was used for the OF and LD tests. The floor of each arm was made of white plastic, and the wall of the closed arms and the ridge of the open arms were made of clear plastic. The closed arms and open arms were arranged orthogonally 60 cm above the floor. The illuminance at the central platform of the maze (5×5 cm) was 70 lx. In the EPM test, mice were individually placed on the central platform facing an open arm and were then allowed to move freely in the maze for 5 min. Total distance traveled, % of time spent in the open arms, and number of open arm entries as a percentage of the total number of entries were measured as indices. Data were collected and analyzed by using Image J EPM (O'Hara).

Inanimate object approach tests

This test was performed in the OF apparatus. A mouse was first placed in the OF with 70 lx illuminance for 15 min (habituation session). After the habituation session, the mouse was returned to its home cage and an inanimate object was placed in the center of the field. In the next test session, the mouse was placed again in the OF with the novel object. The large object was prepared by joining two paper cups by their openings (see Figure 3A). Inside the bottom of one cup, a metal block was placed to give stability, and gray monotone and check-patterned printed papers were wrapped around the external surfaces of the cups. Each large object was discarded after use and a new object that had had no contact with the experimental animals was used. The mean time interval between two sessions was 4 min. The total distance traveled and % of time spent in the central area (30% of the field), which included the object and the area around it, were analyzed by using Image J OF4 (O'Hara). Contacts with the novel object were counted on the video records by an observer who was blind to the genotypes. Contact was defined as a forward movement toward the object and subsequent direct contact using the head.

Novel object recognition test

The experiments were done in accordance with the method of Yoshiike et al. [30]. The test is based on the innate tendency of

rodents to differentially explore novel objects over familiar ones. Briefly, the mice were habituated for 15 min to a cage (17 cm×28 cm×12 cm [H]) without bedding materials. After the habituation session, the mice were exposed to two identical small objects for 15 min (training session). Soon after the training session, the mice were presented again with two objects, one used in the training session and a novel object (test session). The used small objects were spherical, conical, cube-shaped, or columnar, made of metal painted black or white in patterns, and generally consistent in their heights and volumes (Figure 3B). The behavior of the mice was video-recorded and the contact with each object was assessed with the naked eye, as in the inanimate object approach test.

Social discrimination test

This test was performed in the OF test apparatus with 70 lx luminance. The test consisted of a habituation session, first test session, and second test session. Each session continued for 15 min and took place in the following order. In the habituation session, two empty cylindrical wire cages (inner size, 7 cm×15 cm [H]; outer size, 9 cm×16.5 cm [H], with twenty-one 3-mmvertical stainless wires longitudinally and gray polyvinyl discs on the top and the bottom, manufactured by the RIKEN Rapid Engineering Team) were placed in two adjacent corners. In the first test session, a mouse (7-week-old male DBA2, purchased from Nihon SLC, Shizuoka, Japan) that was new to the test mouse was put in one of the two cylindrical cages. In the second test session, another mouse that was also new to the test mouse was put in the remaining cylindrical cage. Between the three sessions there were 4-min intervals, during which the test mouse was returned to its home cage. The three sessions were video-recorded from above, and the times spent in the two corner squares containing the cylinders within the 3- ×3-square subdivision (17.7×17.7 cm square) were measured with Image J OF4 (O'Hara). For the two test sessions, video recording was also done from an obliquely upward position to observe contact between the test mouse and the in-cage mouse. Contact with the in-cage mouse was defined as a forward movement toward the mouse in the cage and subsequent direct contact using the head. The position and posture of the in-cage mouse were observable through the slits of the wires. The contacts were counted on the video records by an observer who was blind to the genotypes. Each in-cage mouse was used once a day; when the habituation session began, the mouse was simultaneously placed in its cylindrical cage on the corners of an OF box that was not being used for the tests. These rules were thought to minimize the difference between the two in-cage mice in the second test sessions in regard to their acclimation to the cylindrical cage and the OF-box environment. After each use, the cylindrical cage was extensively washed with water and rinsed with 90% ethanol, which was then evaporated off, to minimize the effects of remnant materials.

Morris water maze test

A circular maze made of white plastic (1 m diameter, 30 cm depth) was filled with water to a depth of about 20 cm (22 to 23°C). The water was colored by the addition of white paint to prevent the mice from seeing the platform (20 cm high, 10 cm diameter; 1 cm below the surface of water) or other cues under the water. Some extra-maze landmark cues (i.e. a calendar, a figure, and a plastic box) were visible to the mice in the maze. The movements of the mice in the maze were recorded and analyzed with Image J WM (O'Hara). Mice received six trials (= 1 session) per day for 4 consecutive days. Each acquisition trial was initiated by placing an individual mouse into the water facing the outer edge of the maze at one of four designated starting points quasi-randomly; the position of the submerged platform remained constant for each mouse throughout the testing. A trial was terminated when the mouse reached the platform, and the latency and distance swum were measured. The cut-off time of the trial was 60 s; mice that did not reach the platform within 60 s were removed from the water and placed on the platform for 30 s before being toweled off and placed back into their home cages. The inter-trial interval was about 6 min. After 4 days of training, a probe test was conducted on day 5. In the probe test, the platform was taken away; each mouse was placed into the water at a point opposite to the target platform and allowed to swim in the maze for 60 s. The distance swum, the number of crossings of the position of the target platform and the other three platforms, and the time spent in each of the four quadrants were measured.

Classical fear conditioning

This test consisted of three parts: a conditioning trial (Day 1), a context test trial (Day 2), and a cued test trial (Day 3). Fear conditioning was performed in a clear plastic chamber equipped with a stainless-steel grid floor [34×26×30 (H) cm]. A CCD camera was mounted on the ceiling of the chamber and connected to a video monitor and computer. The grid floor was wired to a shock generator. White noise (65 dB) was supplied from a loudspeaker as an auditory cue [i.e. the conditioned stimulus (CS)]. The conditioning trial consisted of a 2-min exploration period followed by two CS–US pairings separated by 1 min. A US (foot-shock: 0.5 mA, 2 s) was administered at the end of the 30-s CS period. Twenty-four hours after the conditioning trial, a context test was performed in the same conditioning chamber for 3 min in the absence of the white noise. A cued test was also performed in an alternative context with distinct cues; the test chamber was different from the conditioning chamber in terms of luminance (about 0 to 1 lx), color (white), floor structure [no grid but with thin bedding material (Alpha-Dri: Shepherd, TN, USA)], and shape (triangular). The cued test was conducted 24 h after the contextual test was finished; it consisted of a 2-min exploration period (no CS) to evaluate nonspecific contextual fear, followed by a 2-min CS period (no foot shock) to evaluate the acquired cued fear. The rate of freezing response (immobility, except for respiration and heartbeat) of mice was measured as an index of fear memory. Data were collected and analyzed with Image J FZ2 (O'Hara).

Acoustic startle response and prepulse inhibition

For startle response testing, each mouse was put into a small cage (30 or 35 mm diameter, 12 cm long) and the cage was placed on a sensor block in a soundproof chamber [60×50×67 cm (H)]. A dim light was mounted on the ceiling of the soundproof chamber (10 lx at the center of the sensor block), and 65-dB white noise was presented as background noise. In the auditory startle response test, mice were acclimatized to the experimental conditions for 5 min, and then the experimental session began. In the first session, 120-dB startle stimuli (40 ms) were presented to the mice 10 times, with random inter-trial intervals (10 to 20 s). In the second session, startle responses to stimuli at various intensities were assessed. Five white noise stimuli (each 40 ms) at 70 to 120 dB (70, 75, 80, 85, 90, 95, 100, 110, or 120 dB) were presented in quasi-random order and with random inter-trial intervals (10 to 20 s). In the prepulse inhibition session, mice experienced five types of trial: no stimulus; startle stimulus (120 dB, 40 ms) only; prepulse 70 dB (20 ms, lead time 100 ms) and pulse 120 dB; prepulse 75 dB (20 ms, lead time 100 ms) and pulse 120 dB; and prepulse 80 dB (20 ms, lead time 100 ms) and pulse 120 dB. Each trial was performed 10 times in quasi-random order and with random inter-trial intervals (10 to 20 s). In the final session, a 120-dB

startle stimuli (40 ms) was presented to the mice 10 times with random inter-trial intervals (10 to 20 s). The total duration of an auditory startle response test was about 35 to 40 min. After each trial, the holding chambers were washed with tap water, wiped with a paper towel, and dried. Apparatuses and software used for the data analysis were commercially available ones (Mouse Startle; O'Hara).

Effects of MK-801, clozapine, or fluoxetine administration on animal behaviors

MK-801 (Sigma, St. Louis, MO) was dissolved in saline at a concentration of 0.05 mg/ml and administered to mice intraperitoneally at a dose of 0.5 mg/kg. Clozapine (Sigma) was dissolved in small amount of 1N HCl, pH-adjusted to 5 with 1 N NaOH, diluted to 40 μg/ml with saline, and injected at a dose of 0.4 mg/kg. Fluoxetine hydrochloride (Sigma) was dissolved in saline at a concentration of 1 mg/ml and administered at a dose of 10 mg/kg. Control animals were injected with the same volume of saline. MK-801 treated mice were subjected to the OF test. On the first day, after a 30-min habituation period, the mice were given saline, kept in their home cages for 10 min, and then returned to the OF for a 30-min observation session. On the second day, the same procedure was repeated, with substitution of MK-801 solution for the saline. This was followed by the large inanimate object approach test after a 10-min stay in the home cage. Clozapine or fluoxetine were administered to mice intraperitoneally 30 min before EPM tests. The interval between the clozapine and fluoxetine treatments was 6 days. There was no significant interaction between the two drugs in two-way ANOVA for repeated measurement (data not shown). For the stereotypy-like behavior analysis, the turns were calculated from the X,Y coordinates data provided by Image J OF4 (O'Hara) and rotations were counted in video records by the observer blind to genotypes. A turn was defined by crossing the same standard X or Y positions two times within a second. Nine standard positions were set for both X and Y axes to equally divide the OF area.

Magnetic resonance imaging (MRI) and morphometric analysis

MRI images of adult male mice were acquired by MRI scan using a vertical-bore 9.4-T Bruker AVANCE 400WB imaging spectrometer (Bruker BioSpin, Rheinstetten, Germany). Animals were anesthetized with 3% and 1.5% isoflurane in air (2 L/min flow rate) for induction and maintenance, respectively. MRI images were obtained by using the FISP-3D protocol with Paravision software 5.0 (Bruker BioSpin), with the following parameters: effective echo time = 4.0 ms, repetition time = 8.0 ms, flip angle = 15°, average number = 5, acquisition matrix = 256×256×256, and field of view = 25.6×25.6×25.6 mm. Ten pairs of 36-week-old *Lrrtm1* KO and WT mice were subjected to the analysis. Manual measurements were made of total brain volume, hippocampus volume, and lateral ventricle volume by using Insight ITK-Snap software [4]. Histological examination and immunohistochemical staining were performed as described [31]. Cortical thickness were determined on coronal frozen sections (10 μm, 20 pairs of sections derived from four pairs of *Lrrtm1* KO and WT mice for the prefrontal cortex, motor cortex, and auditory cortex); 50 pairs of sections derived from nine pairs of KO and WT mice were used for the somatosensory cortex.

Golgi staining

Brains from four pairs of 16-week-old *Lrrtm1* KO and WT mice were Golgi-Cox impregnation-stained by using an FD Rapid GolgiStain kit (FD NeuroTechnologies, Ellicott City, MD, USA). Coronal sections 100 μm thick were prepared. Pyramidal neurons that had clear visible staining from the soma to the distal dendrites were randomly selected, and segments (>20 μm) of distal secondary or tertiary dendrites were scanned (53 segments [2294 spines] from four KO mice, 58 segments [2335 spines] from five WT mice) by using a bright-field microscope (Axioskop 2 Plus, Carl Zeiss Japan, Tokyo, Japan) with a 100× objective. Counting of spines (protrusions) and morphometric analysis of spines were performed as described [5]. Individual spines were manually traced by using NeuroLucida software (MBF Bioscience, Williston, VT, USA), and the maximum length and head width of spines were then measured. Means of these parameters were calculated for each segment and compared between genotypes.

Electron microscopic analysis

Anesthetized mice (25 weeks old, 3 pairs of *Lrrtm1* KO and WT) were perfused with 2% paraformaldehyde – 2.5% glutaraldehyde in 0.1 M phosphate buffer (pH 7.4). Brains were sectioned at 500 μm, osmicated with 1% OsO_4 in phosphate buffer, dehydrated through a gradient series of ethanol, and then embedded in epoxy resin (Epon 812, TAAB Laboratories Equipment Ltd., Berkshire, England) by polymerization. Eighty-nanometer-thick ultrathin sections from the hippocampus were cut with an ultramicrotome (Ultracut UCT, Leica Microsystems, Wetzlar, Germany), collected on 200-mesh uncoated copper grids (Maxtaform HF34), and counterstained with uranyl acetate and lead citrate. CA1 stratum radiatum and stratum oriens, in regions about 100 μm apart from the pyramidal cell layer, were examined electron microscopically (Tecnai 12, FEI, Eindhoven, Netherlands). Photographic images were acquired by digital camera (Tem Cam F416, TVIPS, Gauting, Germany) attached to the electron microscope. Mean synaptic densities were calculated by counting asymmetric synapses, which had clear synaptic vesicles with PSD, over an area of more than 10,000 μm^2 per genotype per region (stratum radiatum and stratum oriens), in 2900× images. For the fine structural analysis, we obtained highly magnified photos (9300×). Every asymmetric synapse with clear presynaptic and postsynaptic membranes was manually analyzed by using NeuroLucida software (MBF Bioscience) for synaptic vesicle density, mean distance between synaptic vesicles, synaptic cleft width, PSD length, and PSD thickness (more than 60 synapses per genotype and per region).

Statistics

Statistical analyses were conducted by using the SPSS statistical package (ver. 16.0, SPSS Japan Inc., Tokyo, Japan). Parametric data were analyzed by using Student's *t*-test, and non-parametric data were analyzed by using Mann-Whitney's *U*-test. The *P* values refer to the Student's *t*-test unless otherwise noted. Effects of factors were analyzed by using ANOVAs (Uni-ANOVA, two-way ANOVA with *post hoc* tests and General Linear Model [GLM]). Differences were defined as statistically significant when $P<0.05$.

Supporting Information

Table S1 Summary of Lrrtm1 KO behavioral analysis.
(PDF)

Acknowledgments

We thank Yuji Yoshiike (RIKEN BSI) and Naoko Hara (RIKEN BSI) for their advice on the NOR test and spine morphometric analysis, respectively. We also thank the following RIKEN BSI staff for their technical assistance: Chieko Nishioka, Yayoi Nozaki, Naoko Yamada, and members of the Support Unit for Animal Experiments.

Author Contributions

Conceived and designed the experiments: NT YSO KS TA TH NM KY JA. Performed the experiments: NT YSO KS TA KY JA. Analyzed the data: NT YSO KS TA TH NM KY JA. Contributed reagents/materials/analysis tools: TH KY JA. Wrote the paper: KS TA TH KY JA.

References

1. Freedman R (2003) Schizophrenia. N Engl J Med 349: 1738–1749.
2. Ross CA, Margolis RL, Reading SA, Pletnikov M, Coyle JT (2006) Neurobiology of schizophrenia. Neuron 52: 139–153.
3. Arguello PA, Gogos JA (2006) Modeling madness in mice: one piece at a time. Neuron 52: 179–196.
4. Kellendonk C, Simpson EH, Kandel ER (2009) Modeling cognitive endophenotypes of schizophrenia in mice. Trends Neurosci 32: 347–358.
5. Desbonnet L, Waddington JL, Tuathaigh CM (2009) Mice mutant for genes associated with schizophrenia: common phenotype or distinct endophenotypes? Behav Brain Res 204: 258–273.
6. Karayiorgou M, Simon TJ, Gogos JA (2010) 22q11.2 microdeletions: linking DNA structural variation to brain dysfunction and schizophrenia. Nat Rev Neurosci 11: 402–416.
7. Francks C, Maegawa S, Lauren J, Abrahams BS, Velayos-Baeza A, et al. (2007) LRRTM1 on chromosome 2p12 is a maternally suppressed gene that is associated paternally with handedness and schizophrenia. Mol Psychiatry 12: 1129–1139, 1057.
8. Ludwig KU, Mattheisen M, Muhleisen TW, Roeske D, Schmal C, et al. (2009) Supporting evidence for LRRTM1 imprinting effects in schizophrenia. Mol Psychiatry 14: 743–745.
9. Lauren J, Airaksinen MS, Saarma M, Timmusk T (2003) A novel gene family encoding leucine-rich repeat transmembrane proteins differentially expressed in the nervous system. Genomics 81: 411–421.
10. Linhoff MW, Lauren J, Cassidy RM, Dobie FA, Takahashi H, et al. (2009) An unbiased expression screen for synaptogenic proteins identifies the LRRTM protein family as synaptic organizers. Neuron 61: 734–749.
11. Jaaro-Peled H, Ayhan Y, Pletnikov MV, Sawa A (2010) Review of pathological hallmarks of schizophrenia: comparison of genetic models with patients and nongenetic models. Schizophr Bull 36: 301–313.
12. Steen RG, Mull C, McClure R, Hamer RM, Lieberman JA (2006) Brain volume in first-episode schizophrenia: systematic review and meta-analysis of magnetic resonance imaging studies. Br J Psychiatry 188: 510–518.
13. Vita A, De Peri L, Silenzi C, Dieci M (2006) Brain morphology in first-episode schizophrenia: a meta-analysis of quantitative magnetic resonance imaging studies. Schizophr Res 82: 75–88.
14. Ellison-Wright I, Glahn DC, Laird AR, Thelen SM, Bullmore E (2008) The anatomy of first-episode and chronic schizophrenia: an anatomical likelihood estimation meta-analysis. Am J Psychiatry 165: 1015–1023.
15. Young JW, Zhou X, Geyer MA (2010) Animal models of schizophrenia. Current topics in behavioral neurosciences 4: 391–433.
16. Jaaro-Peled H, Hayashi-Takagi A, Seshadri S, Kamiya A, Brandon NJ, et al. (2009) Neurodevelopmental mechanisms of schizophrenia: understanding disturbed postnatal brain maturation through neuregulin-1-ErbB4 and DISC1. Trends Neurosci 32: 485–495.
17. Calabrese EJ (2008) An assessment of anxiolytic drug screening tests: hormetic dose responses predominate. Crit Rev Toxicol 38: 489–542.
18. Liljequist S (1991) Genetic differences in the effects of competitive and non-competitive NMDA receptor antagonists on locomotor activity in mice. Psychopharmacology (Berl) 104: 17–21.
19. Qi C, Zou H, Zhang R, Zhao G, Jin M, et al. (2008) Age-related differential sensitivity to MK-801-induced locomotion and stereotypy in C57BL/6 mice. Eur J Pharmacol 580: 161–168.
20. Cao BJ, Rodgers RJ (1997) Dopamine D4 receptor and anxiety: behavioural profiles of clozapine, L-745,870 and L-741,742 in the mouse plus-maze. Eur J Pharmacol 335: 117–125.
21. Cloos JM (2005) The treatment of panic disorder. Curr Opin Psychiatry 18: 45–50.
22. Uz T, Dimitrijevic N, Akhisaroglu M, Imbesi M, Kurtuncu M, et al. (2004) The pineal gland and anxiogenic-like action of fluoxetine in mice. Neuroreport 15: 691–694.
23. Siddiqui TJ, Pancaroglu R, Kang Y, Rooyakkers A () Craig AM LRRTMs and neuroligins bind neurexins with a differential code to cooperate in glutamate synapse development. J Neurosci 30: 7495–7506.
24. Powell SB, Zhou X, Geyer MA (2009) Prepulse inhibition and genetic mouse models of schizophrenia. Behav Brain Res 204: 282–294.
25. Gaspar PA, Bustamante ML, Silva H, Aboitiz F (2009) Molecular mechanisms underlying glutamatergic dysfunction in schizophrenia: therapeutic implications. J Neurochem 111: 891–900.
26. Gunduz-Bruce H (2009) The acute effects of NMDA antagonism: from the rodent to the human brain. Brain Res Rev 60: 279–286.
27. Association AP (2000) American Psychiatric Association. Diagnostic and Statistical Manual of Mental Disorders DSM-IV-TR (Text Revision).: Washington, DC.
28. Sakai K, Miyazaki J (1997) A transgenic mouse line that retains Cre recombinase activity in mature oocytes irrespective of the cre transgene transmission. Biochem Biophys Res Commun 237: 318–324.
29. Sakatani S, Yamada K, Homma C, Munesue S, Yamamoto Y, et al. (2009) Deletion of RAGE causes hyperactivity and increased sensitivity to auditory stimuli in mice. PLoS One 4: e8309.
30. Yoshiike Y, Kimura T, Yamashita S, Furudate H, Mizoroki T, et al. (2008) GABA(A) receptor-mediated acceleration of aging-associated memory decline in APP/PS1 mice and its pharmacological treatment by picrotoxin. PLoS One 3: e3029.
31. Aruga J, Inoue T, Hoshino J, Mikoshiba K (2002) Zic2 controls cerebellar development in cooperation with Zic1. J Neurosci 22: 218–225.

Biochemical and Biophysical Research Communications 412 (2011) 460–465

Contents lists available at SciVerse ScienceDirect

Biochemical and Biophysical Research Communications

journal homepage: www.elsevier.com/locate/ybbrc

Comparative characterization of *GPRC5B* and *GPRC5C LacZ* knockin mice; behavioral abnormalities in *GPRC5B*-deficient mice

Takamitsu Sano [a,1], Yeon-Jeong Kim [a,1], Eriko Oshima [a], Chika Shimizu [a], Hiroshi Kiyonari [b], Takaya Abe [b], Hideyoshi Higashi [c], Kazuyuki Yamada [d], Yoshio Hirabayashi [a,*]

[a] *Laboratory for Molecular Membrane Neuroscience, Brain Science Institute, RIKEN, Wako-shi, Saitama 351-0198, Japan*
[b] *Laboratory for Animal Resources and Genetic Engineering, RIKEN Center for Developmental Biology, 2-2-3 Minatojima Minamimachi, Chuo-ku, Kobe 650-0047, Japan*
[c] *Division of Glyco-Signal Research Institute of Molecular Biomembrane and Glycobiology, Tohoku Pharmaceutical University, 4-4-1 Komatsushima, Aoba-ku, Sendai, Miyagi 981-8558, Japan*
[d] *Support Unit for Animal Resources Development, Research Resources Center, Brain Science Institute, RIKEN, Wako-shi, Saitama 351-0198, Japan*

ARTICLE INFO

Article history:
Received 22 July 2011
Available online 5 August 2011

Keywords:
GPRC5B
GPRC5C
Central nervous system
Animal behavior

ABSTRACT

Although *GPRC5B* and *GPRC5C* are categorized into the G protein-coupled receptor family C, including glutamate receptors, GABA receptors, and taste receptors, their physiological functions remain unknown. Since both receptors are expressed in the brain and evolutionarily conserved from fly to human, it is conceivable that they have significant biological roles particularly in the central nervous system (CNS). We generated *GPRC5B*- and *GPRC5C*-deficient mice to examine their roles in the CNS. Both homozygous mice were viable, fertile, and showed no apparent histological abnormalities, though *GPRC5B*-deficient mice resulted in partial perinatal lethality. We demonstrated that the expressions of *GPRC5B* and *GPRC5C* are developmentally regulated and differentially distributed in the brain. *GPRC5B*-deficient mice exhibited altered spontaneous activity pattern and decreased response to a new environment, while *GPRC5C*-deficient mice have no apparent behavioral deficits. Thus, *GPRC5B* has important roles for animal behavior controlled by the CNS. In contrast, *GPRC5C* does not affect behavior, though it has a high sequence similarity to *GPRC5B*. These findings suggest that family C, group 5 (*GPRC5*) receptors in mammals are functionally segregated from their common ancestor.

1. Introduction

G protein-coupled receptors (GPCRs) are integral membrane proteins that have seven transmembrane domains [1]. GPCRs recognize various extracellular molecules, including hormones, neurotransmitters, lipids, odors, and pheromones, and transmit signals to the intracellular region through the activation of heterotrimeric G proteins. According to their sequence similarity, GPCRs are largely classified into three families: family A (rhodopsin-like receptors), family B (secretin-like receptors), and family C (metabotropic glutamate receptor-like receptors). Of these, family C is further divided into four subfamilies: group I (calcium-sensing receptors, taste receptors, GPRC6 receptors, and V2R pheromone receptors), group II (metabotropic glutamate receptors), group III (GABA receptors), and group IV (*GPRC5* receptors) [2]. GPCR family C receptors, most of which are expressed in the CNS, characteristically have a long N-terminal domain involved in ligand binding. However, unlike other GPCR family C receptors, *GPRC5* receptors exceptionally have a short N-terminal domain.

The seven transmembrane domains of *GPRC5* receptors are evolutionarily conserved from fly to human. In fly, BOSS is the only ortholog corresponding to *GPRC5* receptors [3]. In contrast, *GPRC5* receptors have four subtypes, *GPRC5A*, *GPRC5B*, *GPRC5C*, and *GPRC5D* in mammals [4–7]. *GPRC5* receptors were originally identified as retinoic acid-induced gene, as named RAIG [6]. Therefore, these receptors are likely to play important roles in embryonic development, differentiation, and tumor formation. In fact, tumor formation in the lung is facilitated in *GPRC5A*-deficient mice [8]. Localization studies of GPRC5 receptors showed that *GPRC5A* is expressed specifically in the lung [5,6,9], *GPRC5B* is expressed in the brain and placenta [5,9–11], *GPRC5C* is expressed in the brain, liver, and kidney [5,9], and *GPRC5D* is expressed especially in the skin [7,9,12]. Such expression profiles of *GPRC5* receptors imply that *GPRC5B* and *GPRC5C* play important roles in neural functions such as transmitter release, neurite extension, axon guidance, neuronal development, and synaptic plasticity. However, their molecular and physiological functions in the CNS remain unclear so far.

Abbreviations: CNS, central nervous system; GPCRs, G protein-coupled receptors.

* Corresponding author. Fax: +81 48 467 6317.
E-mail address: hirabaya@riken.jp (Y. Hirabayashi).

[1] These authors equally contributed to this work.

0006-291X/$ - see front matter © 2011 Elsevier Inc. All rights reserved.
doi:10.1016/j.bbrc.2011.07.118

In this study, we generated *GPRC5B* and *GPRC5C LacZ* knockin mice and characterized their behaviors. We also prepared specific antibodies against *GPRC5B* and *GPRC5C*, which enabled us to investigate their endogenous expressions at protein level. Using these mutant mice and antibodies to *GPRC5B* and *GPRC5C*, we examined their expression patterns in the brain and their expression changes during brain development, by taking advantage of their knockin mice.

2. Materials and methods

2.1. Generation of GPRC5B- and GPRC5C-deficient mice

GPRC5B (Acc. No. CDB0480K: http://www.cdb.riken.jp/arg/mutant%20mice%20list.html) and *GPRC5C* (Acc. No. CDB0485K: http://www.cdb.riken.jp/arg/mutant%20mice%20list.html) deficient mice were generated by targeted insertion with *LacZ* gene as described in Supplementary methods.

2.2. Animals and genotyping

The experimental procedures and housing conditions for mice were approved by the Institute's Animal Experiments Committee. All the animals were cared for and treated humanely in accordance with the Institutional Guidelines for Experiments using animals. All of the mice were housed in animal facility with a 12-h light/12-h dark cycles at constant temperature (23 ± 2 °C). The mice had free to access water and chow diet (CRF-1, Oriental Yeast, Tokyo, Japan). Mutant mouse lines were maintained on C57BL/6J backgrounds, genotyped by PCR (Supplementary methods), and backcrossed with C57BL/6J mice ten times to purify the backgrounds.

2.3. Cell culture and transfection

HEK293T cells were maintained in Dulbecco's modified Eagle's medium supplemented with 10% fetal calf serum, 100 units/ml penicillin, and 100 μg/ml streptomycin. Transfection was performed with the indicated expression plasmids (Supplementary methods) using Xfect transfection reagent (Clontech, Palo Alto, CA, USA) according to manufacturer's instructions.

2.4. Preparation of polyclonal antibodies against mouse GPRC5B v1, GPRC5B v2, and GPRC5C

Rabbit polyclonal antibodies against *GPRC5B v1*, *GPRC5B v2*, and *GPRC5C* were raised against *GPRC5B v1* synthetic peptide (CGGTIPTAPPSHTGRHHW), *GPRC5B v2* synthetic peptide (CGGTEMAVHPRSLESFGAF), or *GPRC5C* synthetic peptide (CDGKISQVFRNPYVWD). The antibody was affinity-purified using the antigen-coupled column chromatography.

2.5. Preparation of tissue homogenates

Male C57BL/6J mice were killed by cervical dislocation. The isolated tissues were briefly rinsed with phosphate-buffered saline (PBS), frozen in liquid nitrogen, and stored at −80 °C. Tissues were homogenized using a Polytron (Kinematica, Littau, Switzerland) in lysis buffer (50 mM Hepes-NaOH, pH 7.5, 150 mM NaCl, 1 mM DTT, 1 mM EDTA, 1 mM PMSF, and 10% glycerol) supplemented with a protease inhibitor cocktail (Complete, Roche Molecular Biochemicals, Mannheim, Germany) and sonicated. The tissue homogenates were then centrifuged at 1000*g* for 3 min at 4 °C to remove debris. The protein concentration was determined by BCA assay kit (Thermo Scientific, Rockford, IL, USA).

2.6. Western blotting

Proteins were subjected to SDS–PAGE and transferred onto Immobilon polyvinylidene difluoride membrane (Millipore, USA). The membrane was blocked in TBS-T (137 mM NaCl, 20 mM Tris–HCl, pH 7.5, and 0.05% Tween 20) containing 5% skimmed milk, and incubated with anti-FLAG, M2 (1 μg/ml, Sigma), anti-α-tubulin (clone DM1A, 1:10,000, Sigma), anti-*GPRC5B v1* (1:3000), anti-*GPRC5B v2* (1:1000), or anti-*GPRC5C* (1:1000) antibodies. The blot was washed with TBS-T and then incubated with HRP-linked anti-mouse or rabbit IgG antibody (1:5000) (Cell Signaling, Beverly, MA, USA). The blot was washed again with TBS-T. The protein was visualized by chemiluminescence using a Chemi-Lumi One reagent (Nacalai Tesque, Kyoto, Japan).

2.7. β-Galactosidase staining

Mice were anaesthetized with sodium pentobarbital (nenbutal; 30–50 mg/kg delivered by intraperitoneal injection) and infused with 4% paraformaldehyde in 0.1 M phosphate buffer (pH 7.4). The tissue was removed, placed in fixative for 1 h, and then equilibrated overnight in 30% sucrose in 0.1 M phosphate buffer. Frozen sagittal sections were prepared at 30 μm of thickness, stained overnight with X-gal (5-bromo-4-chloro-3-indolyl β-galactosidase) (Sigma), and counterstained with eosin.

2.8. Behavioral tests

Homecage activity test, open field test, light/dark transition test, tail flick test, and passive avoidance test were essentially performed as described before [13–15].

2.9. Statistical analysis

The data were presented as means ± S.E.M. and statistically analyzed using two-tailed student's *t*-test and one-way ANOVA with SPSS software (ver. 16, SPSS, Chicago, IL, USA). Significant differences were considered at $P < 0.05$.

3. Results

3.1. Generation of GPRC5B- and GPRC5C-deficient mice

We generated *GPRC5B*- and *GPRC5C*-deficient mice by inserting *LacZ* on the downstream of each translation initiation site in exon 2 (Fig. 1A and B), which enabled us to examine the endogenous *GPRC5B* or *GPRC5C* expression. Genotype of offspring given from heterozygous mice was confirmed by PCR and Southern blotting (Fig. 1C–F). Both offspring of *GPRC5B* and *GPRC5C* mice were birthed in Mendelian ratios (Table 1). Around 30% of *GPRC5B* homozygous mice ($GPRC5B^{-/-}$) resulted in death at postnatal day 0 (P0), though P0 dead pups showed similar body weight between genotypes (Fig. 2). In addition, approximately 50% of $GPRC5B^{-/-}$ mice died before 4 weeks of age. The survived $GPRC5B^{-/-}$ mice were healthy, fertile, and lived to be around 2 years as well as wild-type mice. On the other hand, $GPRC5C^{-/-}$ mice were viable and fertile. There was no distinct tissue abnormality in the brain, lung, kidney, liver, spleen, stomach, and intestine in both homozygous mice (data not shown).

3.2. Spatially and developmentally regulated expressions of GPRC5B and GPRC5C in the brain

We performed X-gal staining to clarify the distributions of *GPRC5B* and *GPRC5C* in the brain (Fig. 3 and summarized in

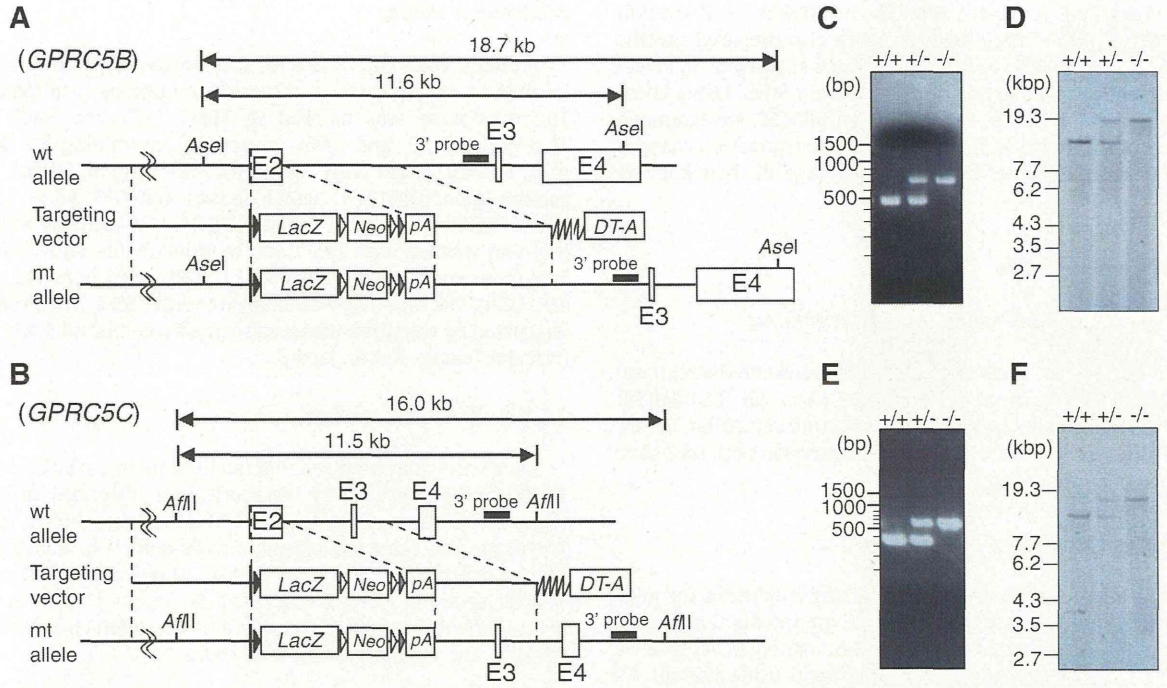

Fig. 1. Generation of *GPRC5B*- and *GPRC5C*-deficient mice. (A and B) Schematic representation of the *GPRC5B* and *GPRC5C* targeting strategy. The structures of the mouse *GPRC5B* and *GPRC5C* loci are shown at the top, the structures of the targeting vector in the middle, and the predicted structures of the homologous recombined locus on the bottom. The β-galactosidase (*LacZ*) reporter gene is under the control of each promoter. The genotype of mouse offspring from heterozygous mating was identified by the PCR amplification of their genomic DNA (C and E), the Southern blot analysis (D and F). DT-A, diphtheria toxin A chain.

Table 1
GPRC5B and *GPRC5C* genotype ratios produced by heterozygous breeding pairs.

	+/+ (%)	+/− (%)	−/− (%)	Unknown[a]
GPRC5B				
Male	37	60	14	
Female	36	63	17	
Mortality from birth until 12 days	4	13	24	11
Total	77	136	55	11
	(27.5)	(48.7)	(19.7)	(3.9)
Expected Mendelian ratios	69.8	139.5	69.8	
	(25)	(50)	(25)	
GPRC5C				
Male	21	39	20	
Female	21	38	20	
Total	42	77	40	
	(26.4)	(48.4)	(25.2)	
Expected Mendelian ratios	39.8	79.5	39.8	
	(25)	(50)	(25)	

[a] Unknown indicates unknown genotype because we failed to collect samples for genotyping.

Table 2). X-gal staining showed that *GPRC5B* was broadly expressed, while *GPRC5C* was distributed in restricted regions in the brain. Interestingly, the distinct difference in localization patterns of *GPRC5B* and *GPRC5C* were observed in the olfactory bulb, the hippocampus, and the cerebellum. In the olfactory bulb, strong staining for *GPRC5B* was observed in the granular cell layer, while *GPRC5C* was distributed in the glomerular layer (Fig. 3B and F). In the hippocampus, *GPRC5B* was expressed highly in the dentate gyrus, and slightly in CA1–CA3 regions, whereas *GPRC5C* was expressed weakly in the CA3 region, but not in the dentate gyrus (Fig. 3C and G). In the cerebellum, *GPRC5B* expression was present in three layers (molecular, Purkinje cell, and granular cell layers), while no *GPRC5C* expression was detected in the Purkinje layer

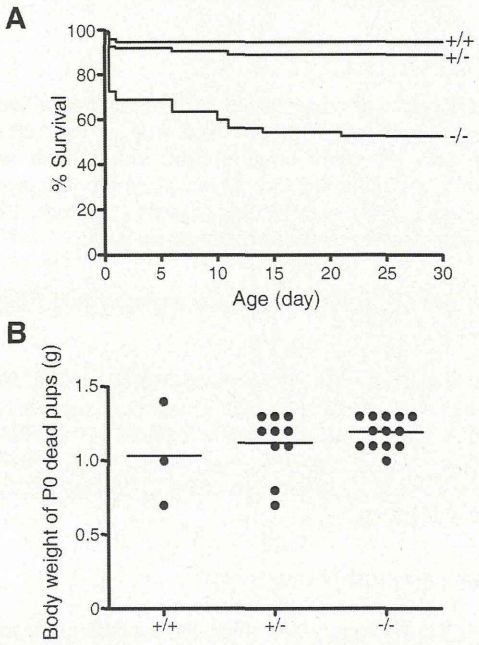

Fig. 2. Partial neonatal lethality of *GPRC5B*-deficient mice. (A) Survival curves of wild-type, *GPRC5B*$^{+/-}$, and *GPRC5B*$^{-/-}$ mice from day 0 to day 30. (B) Body weight of P0 dead pups was measured.

(Fig. 3D and H). Besides these regions, staining for *GPRC5B* was observed moderately in the layer V of the cerebral cortex, hypothalamus, medulla oblongata, pons, slightly in the thalamus (Fig. 3A and Table 2). These results clearly showed that the

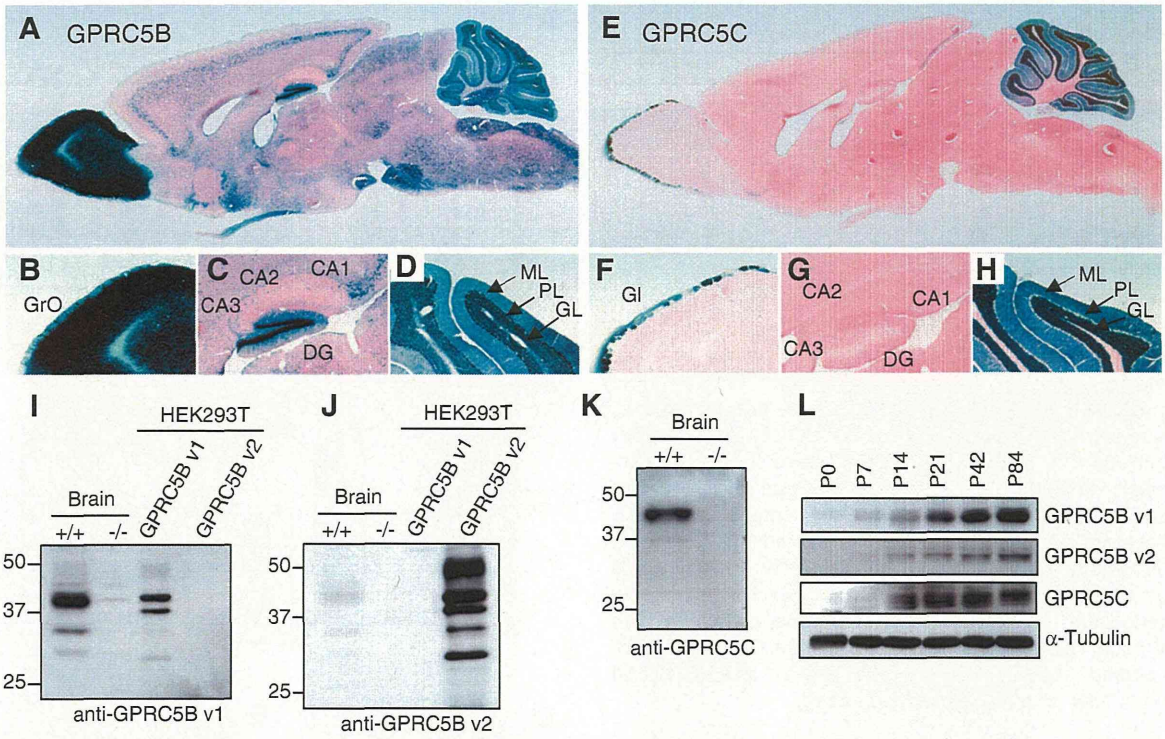

Fig. 3. *GPRC5B* and *GPRC5C* are spatially and developmentally regulated in the brain. X-gal staining of a sagittal brain section (30 μm) from *GPRC5B*$^{+/-}$ knockin mice (A), or *GPRC5C*$^{+/-}$ mice (E) was performed. No staining could be detected in sections from wild-type mice. Enlarged images of the olfactory bulb (B and F), the hippocampus (C and G), or the cerebellum (D and H) were shown. Brain lysates (20 μg) prepared from wild-type, GPRC5B$^{-/-}$, or GPRC5C$^{-/-}$ mice, and total lysates (2 μg) from HEK293T cells expressing *GPRC5B v1*–3xFLAG or *GPRC5B v2*–3xFLAG, were immunoblotted with anti-*GPRC5B v1* (I), anti-*GPRC5B v2* (J), or anti-*GPRC5C* antibodies (K). (L) Brain lysates from P0, P7, P14, P21, P42, or P84 wild-type mice (C57BL/6J background) were immunoblotted using anti-*GPRC5B v1*, anti-*GPRC5B v2*, anti-*GPRC5C* or, to demonstrate uniform protein loading, anti-α-tubulin antibodies. DG, dentate gyrus; Gl, glomerular layer of olfactory bulb; GL, cerebellar granular layer; GrO, granular cell layer of olfactory bulb; ML, cerebellar molecular layer; PL, cerebellar Purkinje layer.

expression of *GPRC5B* and *GPRC5C* were spatially and differentially regulated in the brain.

More recently, novel splice variant of *GPRC5B*, *GPRC5B v2*, was discovered through cDNA microarray and RT-PCR analysis of 97FE65 null mice [16]. The sequence of *GPRC5B v2* differs from that of *GPRC5B v1*, the original *GPRC5B*, at C termini. Interestingly, *GPRC5B v1* exhibits ubiquitous expression, while *GPRC5B v2* shows exclusive expression in the brain [16]. However, expression analysis of *GPRC5B* splicing variants has been studied so far only at mRNA level (Supplementary Fig. S1). Therefore we performed expression analysis of *GPRC5B v1* and *GPRC5B v2* in the brain at protein level. *GPRC5B v1* and *GPRC5B v2* proteins were detected with our each specific antibody, but *GPRC5B v2* protein was barely detectable level with anti-*GPRC5B v2* antibody (Fig. 3I and J). The specificity of each antibody was confirmed by using lysates from HEK293T cells transfected with *GPRC5B v1* or *GPRC5B v2* (Supplementary Fig. S2). *GPRC5C* shares high similarity with *GPRC5B* and is expressed moderately in the brain, as confirmed in Fig. 2K, and highly in peripheral tissues [5,9]. Therefore, we next examined expressions of *GPRC5B* and *GPRC5C* during brain development. As shown in Fig. 2L, expression of *GPRC5B v1* and *GPRC5B v2* were increased in P14 and reached maximum levels in P42, whereas *GPRC5C* expression was increased in P14 and stayed relatively constant until P84. These results indicated that expressions of both *GPRC5B* and *GPRC5C* were developmentally regulated in the brain.

3.3. Behavioral analysis of GPRC5B- and GPRC5C-deficient mice

Separated expression patterns of *GPRC5B* and *GPRC5C* in the brain regions prompted us to examine whether there was a significant difference in behavior. To address this issue, we performed behavioral analysis including a homecage activity test, an open field test, a light/dark transition test, a tail flick test, and a passive avoidance test for each homozygous mouse. *GPRC5B*$^{-/-}$ mice showed significant difference in a homecage activity test and an open field test, compared with wild-type mice, whereas

Table 2
Relative expression of *GPRC5B* and *GPRC5C* in the brain.

	GPRC5B	*GPRC5C*
Cerebellum		
Purkinje layer	+++[a]	–
Granular layer	+++	+++
Molecular layer	++	++
Cerebral cortex		
Layer V	++	–
Hippocampus		
CA1	±	–
CA2	±	–
CA3	±	+
Dentate gyrus	+++	–
Hypothalamus	++	–
Medulla oblongata	++	–
Olfactory bulb		
Granular layer	+++	–
Glomerular layer	–	+++
Pons	++	–
Thalamus	+	–

[a] Strength of X-gal staining was evaluated in five grades (–, ±, +, ++, +++).

Table 3
Summary of behavioral analysis of *GPRC5B* and *GPRC5C* homozygous mice.

Behavioral analysis	*GPRC5B*$^{-/-}$	*GPRC5C*$^{-/-}$
Homecage activity test	Reduced spontaneous activity before light onset	n.s.[a]
Open field test	Decreased total distance and increased total center time	n.s.
Light/dark transition test	n.s.	n.s.
Tail flick test	n.s.	n.s.
Passive avoidance test	n.s.	n.s.

[a] n.s. stands for not significant.

GPRC5C$^{-/-}$ mice did not show any behavioral impairment in all tests (Table 3). Daily spontaneous activity of wild-type mice showed diurnal rhythm with low activity during the light phase and high activity during the dark phase. Also, during the dark phase, there were two peaks, one after dark onset and the other before light onset. Interestingly, *GPRC5B*$^{-/-}$ mice showed less active, especially before light onset, than wild-type mice (Fig. 4A–C). In open field test, mice were placed in the center of open field, and total center time and distance were measured (Fig. 4D and E). This test is commonly used test for evaluating anxiety in a new and unfamiliar environment. *GPRC5B*$^{-/-}$ mice displayed decrease in total distance and increase in total center time, compared with wild-type mice. These results demonstrated that *GPRC5B*$^{-/-}$ mice showed altered spontaneous activity pattern and decreased response in a new or unfamiliar environment.

4. Discussion

In the present study, we generated and characterized homozygous *GPRC5B*- and *GPCR5C*-deficient mice. *GPRC5B* shares high similarity with *GPRC5C*, though both distributions were largely different in the brain (Fig.3 A–H and Table 2). *GPRC5B* was broadly expressed in the brain with strong staining detected in the olfactory bulb, hippocampus, and cerebellum, whereas *GPRC5C* expression was confined to the glomerular layer of olfactory bulb, hippocampal CA3 region, and the molecular and granular layers of the cerebellum. These observations essentially coincided with previous data with anti-*GPRC5B* antibody [10] and *in situ* hybridization results from the Allen Brain Atlas [17]. Comparing the distribution between *GPRC5B* and *GPRC5C*, *GPRC5B* was separately localized from *GPRC5C*, while partially overlapped localization was observed in a particular region. From the high homology between *GPRC5B* and *GPRC5C*, they are thought to have common or similar functions. Therefore, it is conceivable that *GPRC5B* and *GPRC5C* have complementary function in the hippocampal CA3 region, and region-specific function in the olfactory bulb and Purkinje cells. Alternatively, at regions where *GPRC5B* and *GPRC5C* are colocalized, they might form a heterodimer, which might result in modified functions, as demonstrated by previous studies of $GABA_B$ receptor ($GABA_BR1$+$GABA_BR2$) [18–20] and taste receptors (T1R+T2R and T2R+T3R) [21–23].

We prepared specific antibodies against *GPRC5B v1* and *GPRC5B v2* (Fig. 3 I–K), which enabled us to investigate their endogenous expressions at protein level. Immunoblot analysis of brain lysates showed that expression of *GPRC5B v1* was much higher than that of *GPRC5B v2* in C57BL/6J brain, considering that same amounts (2 μg) of total lysates from HEK293T cells transfected with *GPRC5B v1* or *GPRC5B v2* were loaded onto the gel (Fig. 3I and J). This result differs from recently published data that *GPRC5B v2* was expressed predominantly in C57BL/6J brain [16]. One possible reason for disagreement is that *GPRC5B v2* protein might be unstable and rapidly degraded in the brain. Another reason may be attributed to the difference of the techniques used for detection of *GPRC5B* expression or the problem of primer accessibility or elongation efficiency between *GPRC5B v1* and *GPRC5B v2* primer sets in RT-PCR analysis.

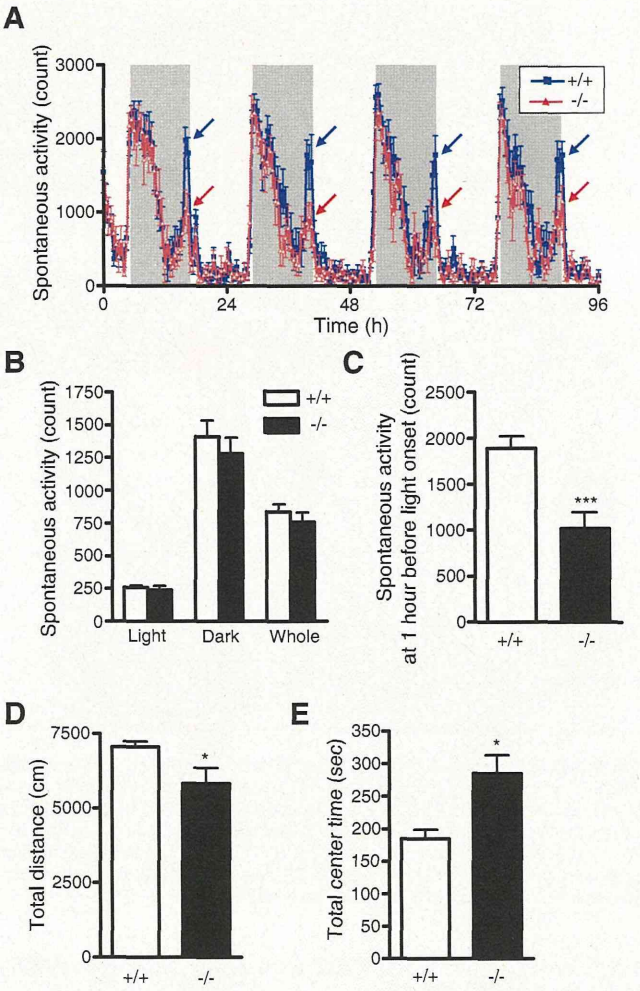

Fig. 4. Altered spontaneous activity pattern and decreased response in unfamiliar circumstance in *GPRC5B*-deficient mice. (A) Spontaneous activity was recorded every 30 min for 96 h. Arrow indicates the time point of 1 h before light onset. Spontaneous activities during light and dark phase, during the whole day (B), and at 1 h before light onset (C) were shown in wild-type (open column) and *GPRC5B*$^{-/-}$ (filled column) mice. Total distance (D) and total center time (E) were measured in open field test. Data represent means ± S.E.M. $^*P < 0.05$, $^{***}P < 0.001$, compared with wild-type mice ($n = 10$ for each genotype).

Our behavior analysis clarified that *GPRC5B*$^{-/-}$ mice showed some behavioral abnormalities (Fig.4). On the other hand, *GPRC5C*$^{-/-}$ mice did not show any distinct behavioral phenotypes involved in brain function, but some abnormality was observed in comprehensive behavior analysis by Japan Mouse Clinic [24]. *GPRC5C*$^{-/-}$ mice exhibited increase in absolute number of reticulocytes, percents of reticulocytes, mean corpuscular volume (MCV), and a percent of basophils (BASO), and decrease in mean corpusculat hemoglobin concentration (MCHC), which suggests that *GPRC5C* deletion affects the regulation of hematopoietic system. In addition, examination of blood chemistry indicated that alkaline phophatase (ALP) and lactic dehydrogenase (LDH), both of which are a general indicator of hepatic damage, were increased in *GPRC5C*$^{-/-}$ mice. In fact we found that *GPRC5C* is expressed in the liver (data not shown), as reported previously [5,7,9,25]. These observations raise the possibility that *GPRC5C* might play important role in regulation of hematopoietic system and liver function.

Acknowledgments

We thank Mr. K. Kamewada, Ms. Y. Shinoda, and Ms. T. Shimizu (RIKEN BSI) for technical assistance. We are also grateful to Japan Mouse Clinic, RIKEN BioResource Center, for help with behavioral analysis. This work was supported by a Grant-in-Aid for Young Scientists (B) (20790187) from the Ministry of Education, Culture, Sports, Science and Technology of Japan.

Appendix A. Supplementary data

Supplementary data associated with this article can be found, in the online version, at doi:10.1016/j.bbrc.2011.07.118.

References

[1] K.L. Pierce, R.T. Premont, R.J. Lefkowitz, Seven-transmembrane receptors, Nature Reviews Molecular Cell Biology 3 (2002) 639–650.
[2] T.K. Bjarnadóttir, R. Fredriksson, H.B. Schiöth, The gene repertoire and the common evolutionary history of glutamate, pheromone (V2R), taste(1) and other related G protein-coupled receptors, Gene 362 (2005) 70–84.
[3] A. Kohyama-Koganeya, Y.J. Kim, M. Miura, Y. Hirabayashi, A Drosophila orphan G protein-coupled receptor BOSS functions as a glucose-responding receptor: loss of boss causes abnormal energy metabolism, Proceedings of the National Academy of Sciences of the United States of America 105 (2008) 15328–15333.
[4] H. Bräuner-Osborne, P. Krogsgaard-Larsen, Sequence and expression pattern of a novel human orphan G-protein-coupled receptor, GPRC5B, a family C receptor with a short amino-terminal domain, Genomics 65 (2000) 121–128.
[5] M.J. Robbins, D. Michalovich, J. Hill, A.R. Calver, A.D. Medhurst, I. Gloger, M. Sims, D.N. Middlemiss, M.N. Pangalos, Molecular cloning and characterization of two novel retinoic acid-inducible orphan G-protein-coupled receptors (GPRC5B and GPRC5C), Genomics 67 (2000) 8–18.
[6] Y. Cheng, R. Lotan, Molecular cloning and characterization of a novel retinoic acid-inducible gene that encodes a putative G protein-coupled receptor, Journal of Biological Chemistry 273 (1998) 35008–35015.
[7] H. Bräuner-Osborne, A.A. Jensen, P.O. Sheppard, B. Brodin, P. Krogsgaard-Larsen, P. O'Hara, Cloning and characterization of a human orphan family C G-protein coupled receptor GPRC5D, Biochimica et Biophysica Acta 1518 (2001) 237–248.
[8] Q. Tao, J. Fujimoto, T. Men, X. Ye, J. Deng, L. Lacroix, J.L. Clifford, L. Mao, C.S. Van Pelt, J.J. Lee, D. Lotan, R. Lotan, Identification of the retinoic acid-inducible Gprc5a as a new lung tumor suppressor gene, Journal of the National Cancer Institute 99 (2007) 1668–1682.
[9] J. Xu, J. Tian, S.D. Shapiro, Normal lung development in RAIG1-deficient mice despite unique lung epithelium-specific expression, American Journal of Respiratory Cell and Molecular Biology 32 (2005) 381–387.
[10] M.J. Robbins, K.J. Charles, D.C. Harrison, M.N. Pangalos, Localisation of the GPRC5B receptor in the rat brain and spinal cord, Brain Research. Molecular Brain Research 106 (2002) 136–144.
[11] S. Imanishi, M. Sugimoto, M. Morita, S. Kume, N. Manabe, Changes in expression and localization of GPRC5B and RARalpha in the placenta and yolk sac during middle to late gestation in mice, Journal of Reproduction and Development 53 (2007) 1131–1136.
[12] S. Inoue, T. Nambu, T. Shimomura, The RAIG family member, GPRC5D, is associated with hard-keratinized structures, Journal of Investigative Dermatology 122 (2004) 565–573.
[13] T. Kato, M. Ishiwata, K. Yamada, T. Kasahara, C. Kakiuchi, K. Iwamoto, K. Kawamura, H. Ishihara, Y. Oka, Behavioral and gene expression analyses of Wfs1 knockout mice as a possible animal model of mood disorder, Neuroscience Research 61 (2008) 143–158.
[14] Y. Santo-Yamada, K. Yamada, E. Wada, Y. Goto, K. Wada, Blockade of bombesin-like peptide receptors impairs inhibitory avoidance learning in mice, Neuroscience Letters 340 (2003) 65–68.
[15] S. Sakatani, K. Yamada, C. Homma, S. Munesue, Y. Yamamoto, H. Yamamoto, H. Hirase, Deletion of RAGE causes hyperactivity and increased sensitivity to auditory stimuli in mice, PLoS ONE 4 (2009) e8309.
[16] B.H. Cool, G.C. Chan, L. Lee, J. Oshima, G.M. Martin, Q. Hu, A flanking gene problem leads to the discovery of a Gprc5b splice variant predominantly expressed in C57Bl/6J mouse brain and in maturing neurons, PLoS ONE 5 (2010) e10351.
[17] E.S. Lein, M.J. Hawrylycz, N. Ao, et al., Genome-wide atlas of gene expression in the adult mouse brain, Nature 445 (2007) 168–176.
[18] K. Kaupmann, B. Malitschek, V. Schuler, J. Heid, W. Froestl, P. Beck, J. Mosbacher, S. Bischoff, A. Kulik, R. Shigemoto, A. Karschin, B. Bettler, GABA(B)-receptor subtypes assemble into functional heteromeric complexes, Nature 396 (1998) 683–687.
[19] R. Kuner, G. Köhr, S. Grunewald, G. Eisenhardt, A. Bach, H.C. Kornau, Role of heteromer formation in GABAB receptor function, Science 283 (1999) 74–77.
[20] K.A. Jones, B. Borowsky, J.A. Tamm, et al., GABA(B) receptors function as a heteromeric assembly of the subunits GABA(B)R1 and GABA(B)R2, Nature 396 (1998) 674–679.
[21] G. Nelson, J. Chandrashekar, M.A. Hoon, L. Feng, G. Zhao, N.J. Ryba, C.S. Zuker, An amino-acid taste receptor, Nature 416 (2002) 199–202.
[22] G. Nelson, M.A. Hoon, J. Chandrashekar, Y. Zhang, N.J. Ryba, C.S. Zuker, Mammalian sweet taste receptors, Cell 106 (2001) 381–390.
[23] X. Li, L. Staszewski, H. Xu, K. Durick, M. Zoller, E. Adler, Human receptors for sweet and umami taste, Proceedings of the National Academy of Sciences of the United States of America 99 (2002) 4692–4696.
[24] S. Wakana, T. Suzuki, T. Furuse, K. Kobayashi, I. Miura, H. Kaneda, I. Yamada, H. Motegi, H. Toki, M. Inoue, O. Minowa, T. Noda, K. Waki, N. Tanaka, H. Masuya, Y. Obata, Introduction to the Japan Mouse Clinic at the RIKEN BioResource Center, Experimental Animals 58 (2009) 443–450.
[25] J.B. Regard, I.T. Sato, S.R. Coughlin, Anatomical profiling of G protein-coupled receptor expression, Cell 135 (2008) 561–571.